Microstructural and Mechanical Comparison of Metakaolin Geopolymer vs Cement Composites with Quartz and Polypropylene

Ardalan Aalipour, Azam Moosavi*

Department of Materials Engineering, SR.C., Islamic Azad University, Tehran, Iran

*E-mail:a-moosavi@srbiau.ac.ir

Abstract

This study evaluates the mechanical performance of a metakaolin-based geopolymer matrix reinforced with quartz particles and polypropylene fibers, in comparison with a Portland cement-based matrix. Compressive strength, shrinkage, and flexural strength tests reveal that incorporating 20 wt% quartz particles significantly improves the mechanical properties of both matrices. The combined use of quartz particles and fibers contributes to shrinkage crack control and dimensional stability through synergistic effects involving particle–matrix interactions, fiber–matrix bonding, fiber surface characteristics, and toughening mechanisms. In the geopolymer matrix, the reinforcement effect of quartz particles is more pronounced due to the formation of a strong and chemically active interfacial bond. Compared with Portland cement composites, quartz particles increase the flexural and compressive strengths of geopolymer composites by approximately 2.5 and 1.3 times, respectively. The addition of 0.5 wt% polypropylene fibers slightly reduces strength but enhances energy absorption and alters the failure mode from brittle to more ductile. Overall, the results highlight the role of fibers in suppressing or arresting brittle fracture in cementitious and geopolymeric composites.

Keywords: Geopolymer; Quartz sand; Portland cement; Polypropylene fiber; Mechanical properties; Microstructure

1. Introduction

Aluminosilicate-based binders, known as geopolymers (G), have emerged as sustainable alternatives to Ordinary Portland cement (OPC) due to their substantially lower CO_2 emissions and reduced thermal

[DOI: 10.22068/ijmse.4372]

energy requirements [1–4]. Unlike OPC, geopolymers do not require calcium carbonate calcination, resulting in lower energy consumption and reduced greenhouse gas release. These “green cements” exhibit excellent mechanical strength, as well as superior resistance to acidic and corrosive environments, abrasion, and high temperatures [4–7].

While OPC benefits from a standardized formulation process, there is no universally accepted mix design for geopolymers. Geopolymerization begins with the dissolution of aluminosilicate precursors in an alkaline activator, producing silicate and aluminate monomers (Si-O and Al-O). These subsequently form oligomers (Si-O-Al), which polymerize into a hardened gel through structural rearrangement, water (H) release, and polycondensation into long-chain polymers [1,8,9]. The primary binding phase in geopolymers is typically a Na/K–Al–Si–H gel, in contrast to the calcium silicate hydrate (C–S–H) phase formed during OPC hydration. Despite these differences, geopolymers, similar to OPC-based systems, are susceptible to considerable drying shrinkage, which may restrict their structural applicability and long-term durability [10].

Previous studies have demonstrated that the incorporation of fine aggregates can effectively reduce drying shrinkage while improving the microstructural density and mechanical performance of both OPC and geopolymer composites [11,12]. In parallel, the inclusion of discrete fibers within brittle cementitious matrices is a well-established strategy to enhance toughness, crack resistance, and post-cracking behavior by restricting crack initiation and propagation under mechanical loading or shrinkage-induced stresses [13,14]. The ambient-temperature synthesis of geopolymers further enables the use of a wide range of metallic and non-metallic fibers, including polyethylene (PE), polypropylene (PP), polyvinyl alcohol (PVA), and nylon fibers [13–20].

Among synthetic fibers, polypropylene fibers are widely used due to their chemical stability, resistance to alkaline environments, low density, and cost-effectiveness**.** However, their relatively smooth and hydrophobic surface may limit interfacial bonding with cementitious and geopolymer matrices, potentially influencing their effectiveness in crack control and shrinkage mitigation [20–22]. Although PP fibers have been shown to modify fracture behavior and improve ductility in OPC-based composites, their microstructural role and reinforcing efficiency in geopolymer matrices remain less clearly

[DOI: 10.22068/ijmse.4372]

understood. In particular, systematic comparisons between PP fiber-reinforced geopolymer and OPC composites are scarce, and the differences in fiber–matrix interaction mechanisms have not been comprehensively clarified.

In this study, the effects of polypropylene fiber incorporation on the microstructural characteristics, drying shrinkage behavior, and mechanical performance of metakaolin-based geopolymer composites are systematically investigated. For direct comparison, analogous fiber-reinforced OPC composites are also examined under identical experimental conditions. By explicitly addressing the existing knowledge gap regarding the role of PP fibers in geopolymer systems relative to conventional OPC matrices, this work aims to contribute to the development of durable, ductile, and environmentally sustainable cementitious materials.

2. Experimental details

2.1. Materials

2.1.1. Geopolymer composite

Following previous studies [23], a potassium-based geopolymer with the molar composition $Al_2O_3 \cdot 3.5SiO_2 \cdot K_2O \cdot 10.5H_2O$ was synthesized. The aluminosilicate precursor was a high-reactivity calcined clay (Metacem, India) with a bulk density of 2.6 g/cm³, an average particle size of 5 μm, and a specific surface area of 20 m²/g. Amorphous microsilica powder (Azna Company, Iran), potassium hydroxide flakes (KOH, 98%), and distilled water were used to prepare a potassium silicate solution with the composition $K_2O \cdot 1.5SiO_2 \cdot 10.5H_2O$.

Quartz sand (99.4% SiO_2, $D_{90} < 200$–250 μm) was supplied by Hamadan Silica Company (Iran). Silica particles served as an inert filler to enhance matrix strength and mitigate drying shrinkage. The chemical compositions of metakaolin, microsilica, and quartz sand—provided by the manufacturers and confirmed by X-ray fluorescence (XRF)—are summarized in Table 1. Their phase compositions, analyzed by X-ray diffraction (XRD), are presented in Fig. 1.

[DOI: 10.22068/ijmse.4372]

Table 1. Chemical composition (XRF) of the metakaolin, microsilica and quartz sand (wt%)

Chemical	SiO_2	Al_2O_3	CaO	Fe_2O_3	TiO_2	MgO	Na_2O	K_2O	SO_3	Cl	C	Si
Metakaolin	53	45	0.09	0.9	0.65	0.03	0.10	0.03	-	-	-	-
Microsilica	96.40	1.32	0.49	0.87	-	0.97	0.31	1.01	0.10	0.04	0.30	0.50
Quartz sand	99.4	0.24	0.09	0.04	-	-	-	-	-	-	-	-

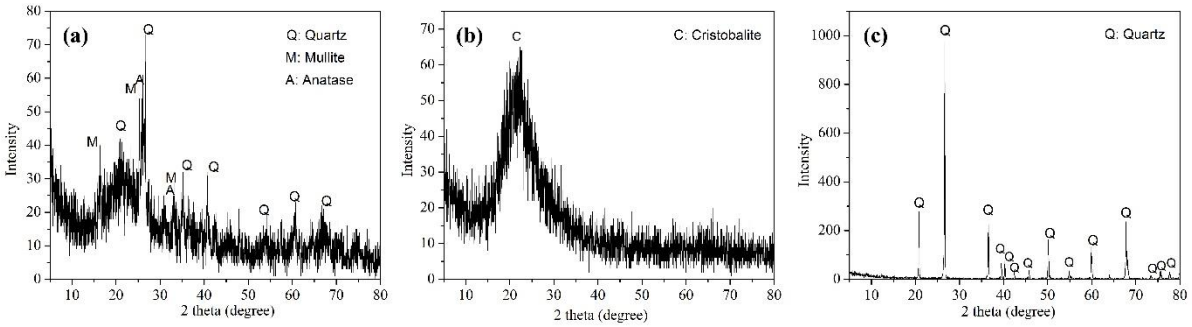

Fig. 1. XRD patterns of (a) metakaolin, (b) microsilica and (c) quartz sand

The XRD pattern of metakaolin revealed a predominantly amorphous phase, indicated by a broad hump between 2θ = 15° and 35°, with crystalline impurities including quartz (JCPDF: 00-002-0458), minor mullite (JCPDF: 00-001-0613), and anatase (JCPDF: 01-089-4203). Microsilica, a by-product of silicon and ferrosilicon production, consisted of over 90 wt% amorphous SiO_2. Quartz sand exhibited a high crystalline silica content and remained chemically inert during geopolymerization.

Polypropylene (PP) fibers were supplied by Iran Concrete Clinic. Their physical and mechanical properties, as reported by the manufacturer, are listed in Table 2. Surface morphologies of quartz sand and PP fibers, observed via scanning electron microscopy (SEM), are shown in Fig. 2. The SEM images indicate that quartz sand possesses an irregular, rough surface with angular edges—likely resulting from mechanical milling—potentially enhancing interfacial bonding with the matrix. In contrast, PP fibers display smooth surfaces, which may reduce fiber–matrix adhesion.

[DOI: 10.22068/ijmse.4372]

Table 2. Physical and mechanical properties of PP fibers

Fiber	Density (g/cm^3)	Length (mm)	Diameter (μm)	Tensile strength (MPa)	Elongation (%)	Melting temp.(°C)
PP	0.91	6	12	400	80	165

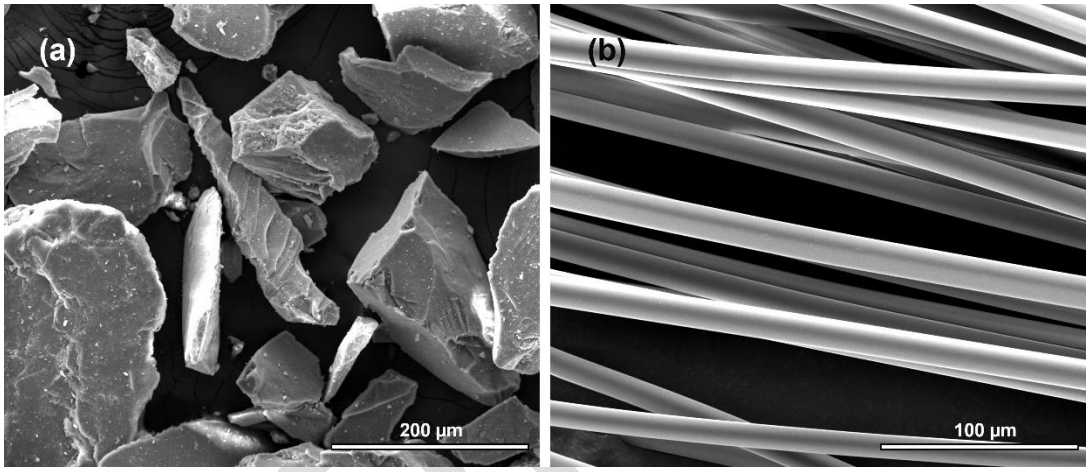

Fig.2. SEM images of (a) quartz sand and (b) PP fiber

2.1.2. Portland cement composite

Type I Portland cement (Grade 425) manufactured by Shahrekord Cement Company (Iran) was used for the preparation of the Portland cement-based composites. According to the manufacturer, this cement complies with the requirements of blended cements under the TS 197-1:2011 standard and is widely used for general construction purposes, particularly in hot climates, due to its favorable workability and versatility.

The X-ray diffraction (XRD) pattern of the as-received Portland cement (Fig. 3(a)) confirms the presence of the principal crystalline phases: tricalcium silicate (C_3S, Ca_3SiO_5, JCPDF: 00-042-0551), dicalcium silicate (C_2S, Ca_2SiO_4, JCPDF: 00-023-1043), tricalcium aluminate (C_3A, $Al_2Ca_3O_6$, JCPDF: 00-038-1429), and tetracalcium aluminoferrite (C_4AF, $Ca_4Al_2Fe_2O_{10}$, JCPDF: 00-010-0032).

Upon the addition of water, hydration reactions are initiated, primarily involving the C_3S and C_3A phases. These exothermic reactions lead to the formation of calcium silicate hydrate (C–S–H) gel—the

[DOI: 10.22068/ijmse.4372]

main binding phase responsible for strength development—and crystalline calcium hydroxide ($Ca(OH)_2$, CH, JCPDF: 00-004-0733) as a byproduct. The XRD pattern of hydrated Portland cement (Fig. 3(b)) shows distinct CH peaks and a broad hump in the 2θ range of 25°–35°, characteristic of the amorphous C–S–H phase [24-26].

While C–S–H gel imparts strength and durability to the cement matrix, CH plays a dual role: it maintains the high alkalinity required for passivation of embedded steel but can also contribute to efflorescence and chemical degradation under aggressive environmental conditions [25-28]. Therefore, the relative content and stability of these phases are critical to the long-term performance of cement-based materials.

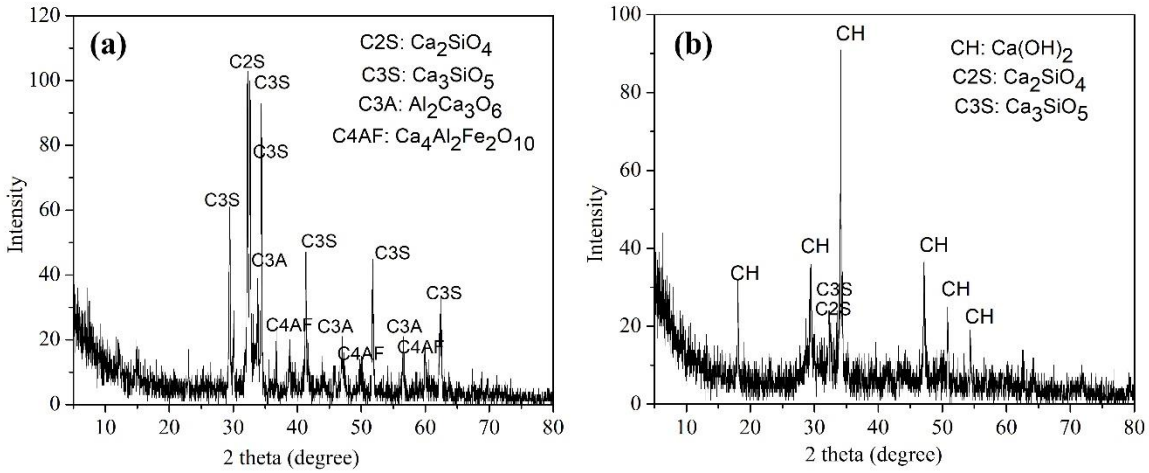

Fig. 3. XRD patterns of (a) Portland cement and (b) hydrated Portland cement

2.2. Mixing and curing

2.2.1. Geopolymer composite

The alkaline silicate solution was prepared by dissolving pre-weighed potassium hydroxide pellets in distilled water under magnetic stirring at 300 rpm. As the dissolution process is exothermic, the solution was allowed to cool to room temperature until fully transparent. Microsilica was then added and mixed for 1 h at 600 rpm to obtain a homogeneous solution, after which metakaolin was incorporated and

[DOI: 10.22068/ijmse.4372]

stirred for 30 min using a mechanical mixer [23]. For the geopolymer mixes, the term “dry mix” refers to the combined mass of metakaolin, microsilica, and KOH flakes before adding distilled water.

Quartz sand (S_X, X = 10, 15, 20, and 25 wt% of the dry mix) was subsequently added and manually mixed for 5 min. The resulting geopolymer concrete slurry was poured into plastic molds with dimensions of 5 × 5 × 5 cm³ and 15 × 15 × 60 mm³. Curing was conducted in an oven at 65 °C for 2 h, followed by 15h at ambient temperature, and a further 15 h at 65 °C.

For the preparation of fiber-reinforced geopolymer composites, polypropylene fibers (F_Y, Y = 0.25, 0.5, 1, and 1.25 wt% of the dry mix) were dispersed in distilled water to prevent agglomeration. The fiber suspension was passed through a graded sieve, oven-dried at 60 °C, and gradually added to the geopolymer slurry over 5 min under continuous mixing. Casting and curing procedures were identical to those used for the non-fiber samples. All specimens were tested 28 days after final curing.

2.2.2. Portland cement composite

Portland cement powder was mixed with quartz sand (S_X, X = 10, 15, 20, and 25 wt% of cement mass) for 5 min using a mechanical stirrer. Distilled water (water-to-cement ratio = 0.5) was then added gradually and the mixture stirred for 2 min at low speed. For the Portland cement, “dry mix” refers solely to the mass of cement before distilled water addition.

For fiber-reinforced composites, polypropylene fibers (F_Y, Y = 0.25, 0.5, 1, and 1.25 wt% of cement mass) were pre-dispersed in distilled water, sieved to ensure separation, oven-dried at 60 °C, and slowly incorporated into the cement slurry under hand-mixing for 3 min.

All mixtures were cast into plastic molds with dimensions of 5 × 5 × 5 cm³ and 15 × 15 × 60 mm³. Curing was carried out under laboratory conditions, and specimens were tested for physical, mechanical, and microstructural properties after 28 days.

It should be noted that the curing regimes adopted for the geopolymer specimens (heat curing) and the Portland cement specimens (ambient curing), while standard for each material system, may influence

[DOI: 10.22068/ijmse.4372]

early-age reaction kinetics and microstructural development; this aspect is therefore considered when interpreting the comparative results.

For the reader's convenience, a summary of the mix nomenclature employed throughout this study is provided in Table 3.

Table 3. Description of Specimens

G (geopolymer)	S_X	S: Quartz sand, X: wt % quartz
	F_Y	F: PP fiber, Y : wt % PP fibers
P (Portland cement)	S_X	S: Quartz sand, X: wt% % quartz
	F_Y	F: PP fiber, Y: wt % PP fibers

3. Testing methods

Drying shrinkage was measured 28 days after curing. The initial length (L_i) was recorded immediately after demolding, and the final length (L_f) was recorded after 28 days. The shrinkage percentage was calculated according to Eq. (1):

$$Shrinkage\ \% = \left(\frac{L_f - L_i}{L_i}\right) \times 100 \quad (1)$$

Compressive strength was determined on 50 × 50 × 50 mm³ cubic specimens using a universal testing machine (Gotech 30 T, Taiwan) at a loading rate of 0.5 mm/min, following ASTM C133-97, 28 days after curing.

Flexural strength was evaluated on 15 × 15 × 60 mm³ prism specimens using a three-point bending test according to ASTM C78. The modulus of rupture (MOR) was calculated using Eq. (2):

$$MOR = \frac{3PL}{2bd^2} \quad (2)$$

Where P is the maximum load before failure (N), L is the span length (mm), b is the specimen width (mm), and d is the specimen depth (mm). Each reported value is the average of five specimens. Flexural strength measurements are reported as mean ± standard deviation (n = 5). Pairwise comparisons between geopolymer and Portland cement at each quartz sand content (X) were performed using

[DOI: 10.22068/ijmse.4372]

Welch's t-test. To assess the effect of quartz sand content within each binder, one-way ANOVA was conducted. Corresponding p-values < 0.05 denote statistically significant differences.

Phase analysis was conducted by X-ray diffraction (XRD, Philips PW3710) using Cu K_α radiation (λ = 1.5406 Å), with a scanning range of 5–80° (2θ) and a step size of 0.02°. Powdered specimens were analyzed with an X'Pert Pro MPD diffractometer (Philips, Netherlands).

Microstructural observations were performed using field emission scanning electron microscopy (FE-SEM, MIRA3 TESCAN, Czech Republic). Energy-dispersive X-ray spectroscopy (EDX) was used to identify elemental distributions. All samples were coated with gold prior to imaging, and the accelerating voltage was set to 15 kV.

4. Results and Discussion

4.1. Mechanical Properties

To determine the optimal quartz sand content (S_X) in geopolymer and Portland cement composites, the flexural strength of specimens was evaluated 28 days after curing (Table 4). As shown, incorporating 20 wt% quartz sand yielded the highest flexural strength for both geopolymer and Portland cement matrices. Notably, the flexural strength of GS_{20} was significantly higher than that of PS_{20}.

In the compressive strength test, the geopolymer sample GS_{20} and Portland cement sample PS_{20} exhibited strengths of 69.87 ± 0.12 MPa and 53.45 ± 0.54 MPa, respectively. However, further increases in quartz sand content beyond 20 wt% led to a decline in strength for both matrices, likely due to the insufficient availability of binder to effectively bond the sand particles and create a well-integrated composite [12]. As a result, the insufficient binder to coat the higher amount of quartz particles, the reduced workability of the mixture leading to less effective compaction, and the increased porosity all negatively affect the mechanical performance. Therefore, the chosen percentage represents a balance between maximizing strength and maintaining good workability and compactness. According to Table 5, at all quartz sand levels, the flexural strength of geopolymer concrete is significantly higher than that of Portland cement concrete (Welch's t-test, $p < 0.001$). These results indicate that both binder type and

[DOI: 10.22068/ijmse.4372]

quartz content strongly affect flexural performance, with geopolymer consistently outperforming Portland cement.

Table 4. Flexural strengths (MPa) of geopolymer (GS_X) and Portland cement (PS_X) concretes at different quartz sand contents (X, wt%)

Quartz sand (X=)	0	5	10	15	20	25
G	5.62±0.08	7.81±0.13	8.30±0.24	9.14±0.05	15.36±0.11	13.52±0.05
P	3.23±0.21	4.18±0.11	5.87±0.09	6.03±0.21	6.20±0.82	5.49±0.98

Table 5. T-test comparison between geopolymer (GS_X) and Portland cement (PS_X) at each quartz sand content (X, wt%), results are derived from Table 4

X%	GS_X (mean±SD)	PS_X (mean±SD)	t	p-value
0	5.62±0.08	3.23±0.21	23.78	<0.001
5	7.81±0.13	4.18±0.11	47.66	<0.001
10	8.30±0.24	5.87±0.09	21.20	<0.001
15	9.14±0.05	6.03±0.21	32.22	<0.001
20	15.36±0.11	6.20±0.82	24.76	<0.001
25	13.52±0.05	5.49±0.98	18.30	<0.001

One-way ANOVA revealed that quartz sand content significantly influenced flexural strength in both binders ($p < 0.001$, Table 6).

Table 6. One-way ANOVA of the effect of quartz sand content (X, wt%) within each binder, values are derived from Table 4

Binder	F	p-value
GS_X	4207.33	<0.001
PS_X	24.59	<0.001

[DOI: 10.22068/ijmse.4372]

A larger F-value indicates a stronger overall effect of quartz sand content on flexural strength, reflecting greater differences among the groups.

For samples with the highest mechanical performance, various polypropylene fiber contents (F_Y) were incorporated. The flexural strength results for fiber-reinforced composites ($GS_{20}F_Y$ and $PS_{20}F_Y$) are presented in Table 7. The geopolymer composite $GS_{20}F_{0.5}$ exhibited the highest modulus of rupture (MOR) of approximately 13.11 ± 0.12 MPa, which is just about 2.96 times greater than the MOR of the $PS_{20}F_{0.5}$ composite.

Table 7. Flexural strengths (MPa) of geopolymer ($GS_{20}F_Y$) and Portland cement ($PS_{20}F_Y$) composites at different PP fiber contents (Y, wt%)

PP fiber (Y=)	0	0.25	0.5	1	1.25
GS_{20}	15.36±0.11	12.12±0.02	13.11±0.12	11.62±0.14	9.31±0.54
PS_{20}	6.20±0.82	5.03±0.16	4.42±0.08	3.33±0.64	3.15±0.12

As shown in Table 7, the flexural strength of $GS_{20}F_Y$ was higher than that of $PS_{20}F_Y$ across all PP fiber contents. The statistical significance of these differences is confirmed by Welch's t-test results presented in Table 8 ($p < 0.001$).

One-way ANOVA results (Table 9) indicate that PP fiber content has a significant effect on the flexural strength in both binders. The F-values are higher for $GS_{20}F_Y$ (88.12) than for $PS_{20}F_Y$ (13.45), suggesting that the influence of fiber content is more pronounced in the geopolymer composite.

[DOI: 10.22068/ijmse.4372]

Table 8. T-test comparison of flexural strength (MPa) between geopolymer ($GS_{20}F_Y$) and Portland cement ($PS_{20}F_Y$) at each PP fiber content (Y, wt%), values are derived from Table 7

Y%	$GS_{20}F_Y$(mean±SD)	$PS_{20}F_Y$ (mean±SD)	t	p-value
0	15.36±0.11	6.20±0.82	20.44	<0.001
0.25	12.12±0.02	5.03±0.16	44.11	<0.001
0.5	13.11±0.12	4.42±0.08	48.27	<0.001
1	11.62±0.14	3.33±0.64	25.72	<0.001
1.25	9.31±0.54	3.15±0.12	25.01	<0.001

Table 9. One-way ANOVA of the effect of PP fiber content (Y, wt%) on flexural strength within each binder ($GS_{20}F_Y$ and $PS_{20}F_Y$), results are based on the data reported in Table 7

Binder	F	p-value
$GS_{20}F_Y$	88.12	<0.001
$PS_{20}F_Y$	13.45	<0.001

Figure 4 compares the compressive stress–strain curves of $GS_{20}F_{0.5}$ and $PS_{20}F_{0.5}$ composites with their respective unreinforced concretes, GS_{20} and PS_{20}. The compressive strength increased from 50.88 ± 0.12 MPa for $PS_{20}F_{0.5}$ to 61.75 ± 0.13 MPa for $GS_{20}F_{0.5}$, representing a 21.4% improvement.

Both geopolymer and Portland cement concretes exhibited brittle failure behavior. In contrast, the fiber-reinforced composites showed a more ductile, non-brittle fracture mode. In brittle specimens, failure occurred suddenly and catastrophically, with a sharp load drop immediately after peak stress. However, fiber-reinforced samples displayed an initial elastic region followed by a nonlinear post-peak response characterized by gradual strength reduction and a stable softening branch in the load–displacement curve. This behavior indicates significant fiber–matrix debonding and fiber pull-out mechanisms [14].

The improved post-peak performance is attributed to the polypropylene fibers' ability to absorb energy and redistribute stresses within the matrix, effectively preventing sudden catastrophic failure and

[DOI: 10.22068/ijmse.4372]

enhancing the material's toughness and ductility. Consequently, the addition of polypropylene fibers significantly enhances the post-peak behavior of both geopolymer and Portland cement composites.

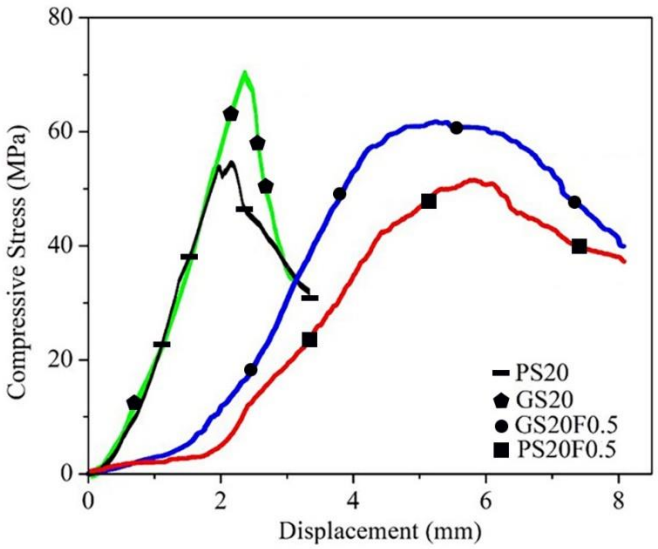

Fig. 4. Effect of PP fiber on compressive curve of geopolymer and Portland cement concretes

4.2. Drying Shrinkage

The linear drying shrinkage percentages of concrete samples containing various amounts of quartz particles are summarized in Table 5. The addition of quartz particles effectively controls shrinkage, which in turn can enhance mechanical properties [12]. Both quartz aggregates and polypropylene fibers play a significant role in reducing longitudinal and volumetric shrinkage in geopolymer composites. Increasing the weight percentage of these reinforcements further mitigates shrinkage, leading to minimized dimensional changes in the composites—a desirable outcome. According to Table 5, geopolymer concretes exhibit higher drying shrinkage compared to Portland cement concretes. This difference is primarily attributed to the greater amount of free water required to improve the workability of the geopolymer slurry, which subsequently evaporates during curing. Unlike Portland cement, where water actively participates in hydration reactions forming C–S–H gels, the excess water in geopolymers does not chemically bond to the aluminosilicate network [12,29-31]. While quartz particles contribute to densifying the microstructure, the shrinkage of the geopolymer matrix remains significantly higher

[DOI: 10.22068/ijmse.4372]

than that of Portland cement. Figure 5 illustrates that the geopolymer composite exhibits approximately 2.5 times greater shrinkage than the Portland cement composite. Nevertheless, the presence of polypropylene fibers effectively controls shrinkage-induced cracking, enhancing dimensional stability. The higher drying shrinkage observed in the geopolymer composites can be directly associated with the development of microcracks within the matrix; the incorporation of polypropylene fibers effectively mitigates this behavior by bridging microcracks and restraining shrinkage-induced crack propagation.

Table 10. Effect of quartz sand content (S_X) on the drying shrinkage (%) of geopolymer and Portland cement matrices

Quartz sand (X=)	0	5	10	15	20	25
G	-2.61±0.12	-1.13±0.30	-0.82±0.24	-0.51±0.23	-0.23±0.01	-0.17±0.03
P	-0.24±0.04	-0.23±0.02	-0.13±0.10	-0.09±0.02	-0.06±0.03	-0.04±0.01

Fig. 5. Visual appearance of $GS_{20}F_{0.5}$ (left) and $PS_{20}F_{0.5}$ (right) composites

4.3. Phase Analysis

Figure 6 presents the X-ray diffraction (XRD) patterns of geopolymer, geopolymer concrete, and geopolymer composite samples. The geopolymer shows typical amorphous characteristics with a broad hump, indicating the loss of crystallinity following the reaction of metakaolin (Fig. 1(a)) with the alkali

[DOI: 10.22068/ijmse.4372]

activator. Both the geopolymer concrete and composite, containing quartz sand and polypropylene fibers, display similar amorphous patterns along with distinct quartz peaks corresponding to the sand particles. The addition of quartz sand and polypropylene fibers does not lead to the formation of any new crystalline phases. This confirms that these reinforcements do not alter the fundamental geopolymer structure or induce crystallization.

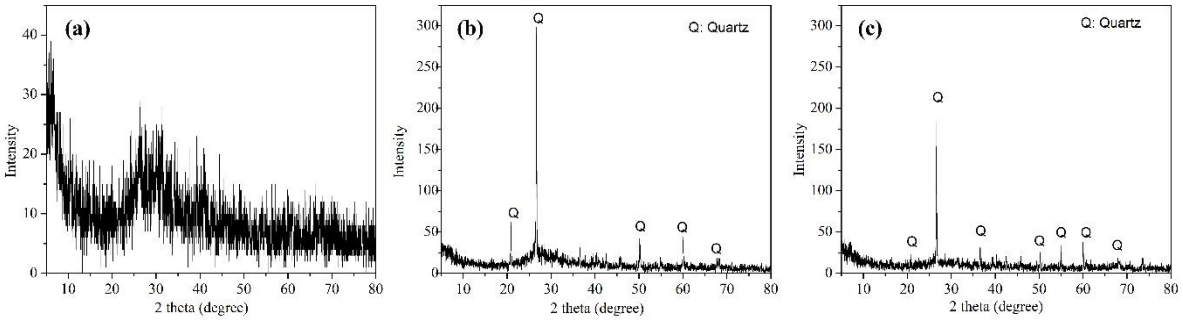

Fig. 6. XRD patterns of (a) geopolymer gel (G), (b) geopolymer concrete (GS_{20}), and (c) geopolymer composite ($GS_{20}F_{0.5}$)

Figure 7 shows the XRD patterns of Portland cement concrete and composite samples. After hydration, characteristic peaks of calcium hydroxide (CH) are observed alongside residual unreacted phases of C_2S and C_3S. During the early hydration stages, cement paste binds the sand particles and imparts initial strength, while over time the formation and interlocking of the amorphous C–S–H network contribute to strength development [25,26]. As C–S–H is amorphous, it does not produce distinct XRD peaks, so only CH and quartz phases are detected. Similar to the geopolymer samples, the addition of quartz sand and polypropylene fibers does not result in new crystalline phases in the Portland cement system.

[DOI: 10.22068/ijmse.4372]

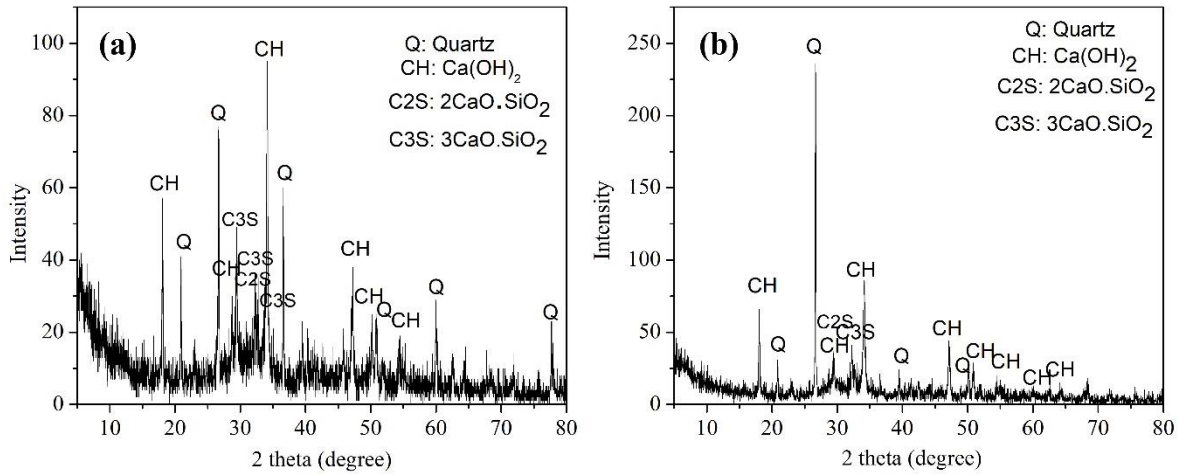

Fig. 7. XRD patterns of (a) Portland concrete (PS_{20}), and (b) Portland composite ($PS_{20}F_{0.5}$)

4.4. Microstructure analysis

The microstructure of geopolymer and Portland cement is shown in Fig. 8. For a more detailed examination, higher magnification images are also presented. The geopolymer in Fig. 8(a) and 8(b) exhibits a homogeneous, relatively dense, and cohesive microstructure. Figure 8(c) shows the C–S–H phase as an amorphous phase exhibiting a sheet-like morphology [27]. Based on the XRD analysis (Fig. 7(b)), which shows distinct peaks corresponding to CH, the observed needle-like crystals can be attributed to calcium hydroxide. In Fig. 8(d), the interconnected, rough-surfaced morphology is characteristic of the typical appearance of C–S–H gel.

[DOI: 10.22068/ijmse.4372]

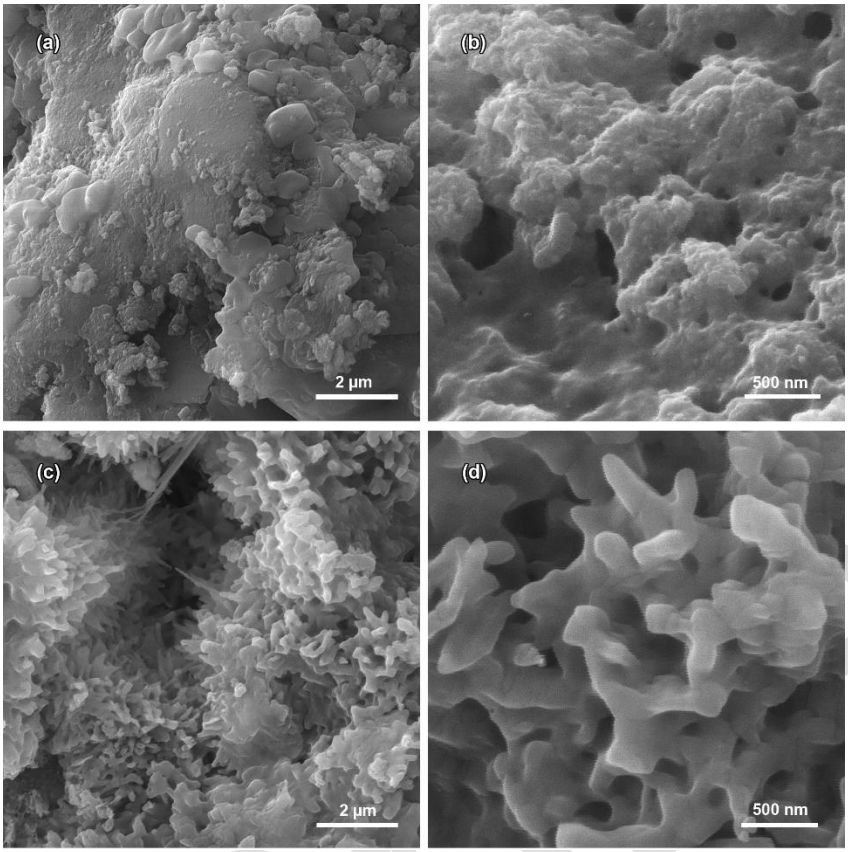

Fig. 8. Microstructure of (a, b) geopolymer and (c, d) hydrated Portland cement with different magnifications

Upon examining the microstructure of the concrete samples, the SEM image and EDX microanalysis in the matrix and sand particles of the GS_{20} and PS_{20} are displayed in Fig. 9. The EDX analysis in Fig. 9(a) reveals that Si, Al, O, and K can be detected in the matrix, consistent with the compositions of geopolymer. Quartz particles did not dissolve in the alkaline media and remained as inert filler within the geopolymer binder. It was observed that the interface between the quartz sand and the matrix in the geopolymer and Portland cement differs. The bond between the reinforcing particles (S) and the geopolymer matrix (M) appears stronger compared to the Portland cement matrix (M). The partial dissolution of quartz particles and the formation of an active interface between the quartz particles and the geopolymer matrix could explain this stronger bond [11,12,32]. Although quartz is commonly considered inert and often remains as filler in geopolymer systems, recent studies challenge this assumption. In particular, the study "Impact of altered quartz surface chemistry on mechanical properties and microstructure of geopolymers" [33] shows that surface activation of quartz (e.g., via

[DOI: 10.22068/ijmse.4372]

mechanical or chemical treatment) generates surface-active groups, such as non-bridging oxygen and silicon radicals. These groups can form Si–O–Si bonds with the surrounding geopolymer gel, significantly reducing interfacial porosity and enhancing mechanical strength. In parallel, molecular level modelling by Kai and Dai [34] demonstrates that at the interface between an aluminosilicate-based geopolymer binder and a silica (quartz) aggregate, Al–O–Si covalent bonds, alkali–O ionic bonds, and hydrogen bonds can form. This results in a dense atomic-level interfacial transition zone rather than a weak, porous layer. Moreover, recent reviews indicate that under alkaline activation, even some crystalline or semi-crystalline phases may partially dissolve or at least undergo surface alteration, thus potentially participating in the geopolymerization process [35]. Taken together, this evidence supports the hypothesis that the observed dense and consistent interface between quartz particles and the geopolymer matrix is not merely due to mechanical interlocking or filler effects. It may also reflect genuine chemical interactions, including the formation of interfacial Si–O–Si and Si–O–Al bonds, and the development of a chemically active interphase. Meanwhile, according to Fig. 9(b), the bond between the quartz particles and the Portland cement matrix is not as well developed. The differences in the microstructure and the interface between the reinforcement and matrix may explain the lower mechanical strength of Portland cement concretes compared to geopolymer concretes, as discussed in section (4.1) mechanical properties. The EDX pattern of the Portland cement matrix shows, in addition to silicon and oxygen, the presence of calcium (Ca) along with iron (Fe), aluminum (Al), and magnesium (Mg), which are key elements in cement compositions and their hydrated products. The EDX pattern of quartz particles, similar to the geopolymer sample, shows peaks of silicon and oxygen. In geopolymer concretes, due to the strong aluminosilicate matrix formed during geopolymerization and its bonding with quartz particles, better mechanical strength was achieved compared to Portland cement concretes.

[DOI: 10.22068/ijmse.4372]

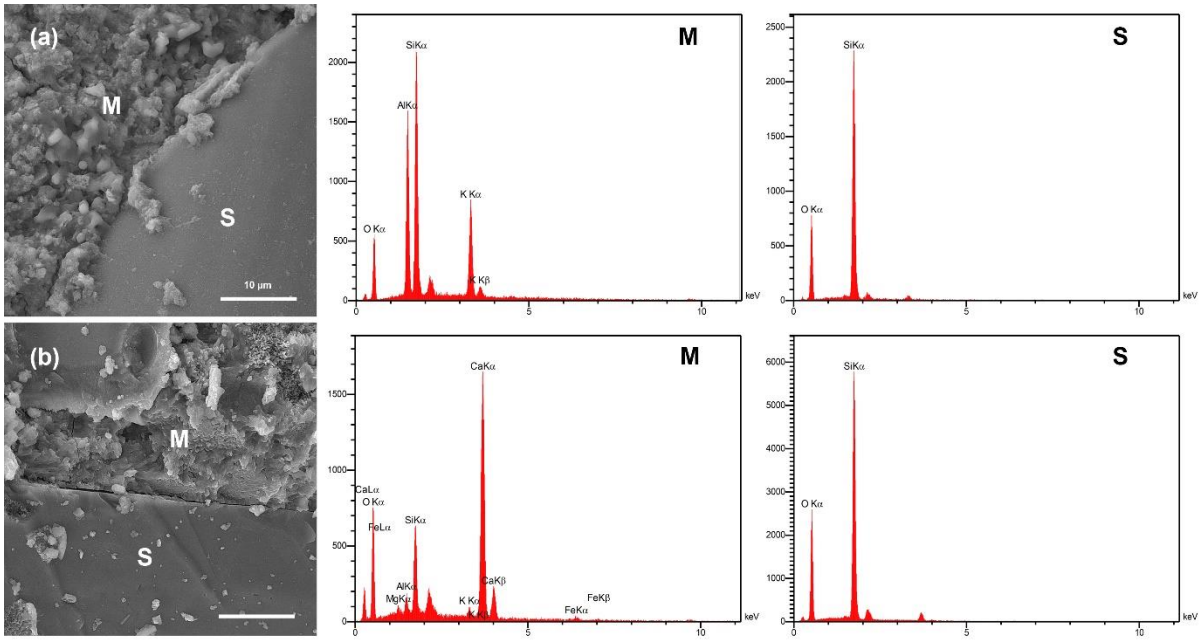

Fig. 9. Microstructure of (a) geopolymer concrete (GS_{20}) and (b) Portland cement concrete (PS_{20}) with EDX patterns of matrix (M) and quartz sand (S)

Figure 10 shows the PP fibers in the geopolymer and Portland cement matrices. This indicates that the surface of the PP fibers differed from that of the original PP fibers (Fig. 2). As seen in Fig. 10(a), a thin layer or coating has formed on the surface of the PP fibers in the geopolymer matrix. EDX analysis of the coating revealed that a higher alkaline geopolymer gel precipitated and adhered to the fiber surface. This indicates alkaline reactions and the formation of a layer of geopolymeric compounds, which could be effective in enhancing the adhesion and mechanical strength of the composites. In contrast, Fig. 10(b) shows fibers with a rougher and scratched surface, indicating surface degradation and visible uneven lines. The fine particles adhered to the surface of the fibers in the EDX analysis suggest slight penetration of calcium silicate products. Presumably, since Portland cement particle sizes are coarser and larger compared to the geopolymer gel, the fiber surface in the cement matrix exhibits more roughness and scratches. The weak PP fiber–geopolymer interface can be explained by the dominance of mechanical interlocking over chemical bonding. Although a thin geopolymer coating is observed on PP fibers (Fig. 10a), PP is chemically inert, has very low surface energy, and lacks functional groups capable of forming strong covalent or ionic bonds with aluminosilicate gel. As a result, chemical adhesion is weak and the coating adheres mainly through physical forces [14]. In contrast, the scratched

[DOI: 10.22068/ijmse.4372]

PP surface in Portland cement (Fig. 10b) provides micro-asperities that significantly enhance mechanical interlock, a mechanism known to govern PP fiber bonding in cementitious composites. Thus, the weaker bond in the geopolymer system arises from limited chemical interaction and lower mechanical interlocking compared to Portland cement.

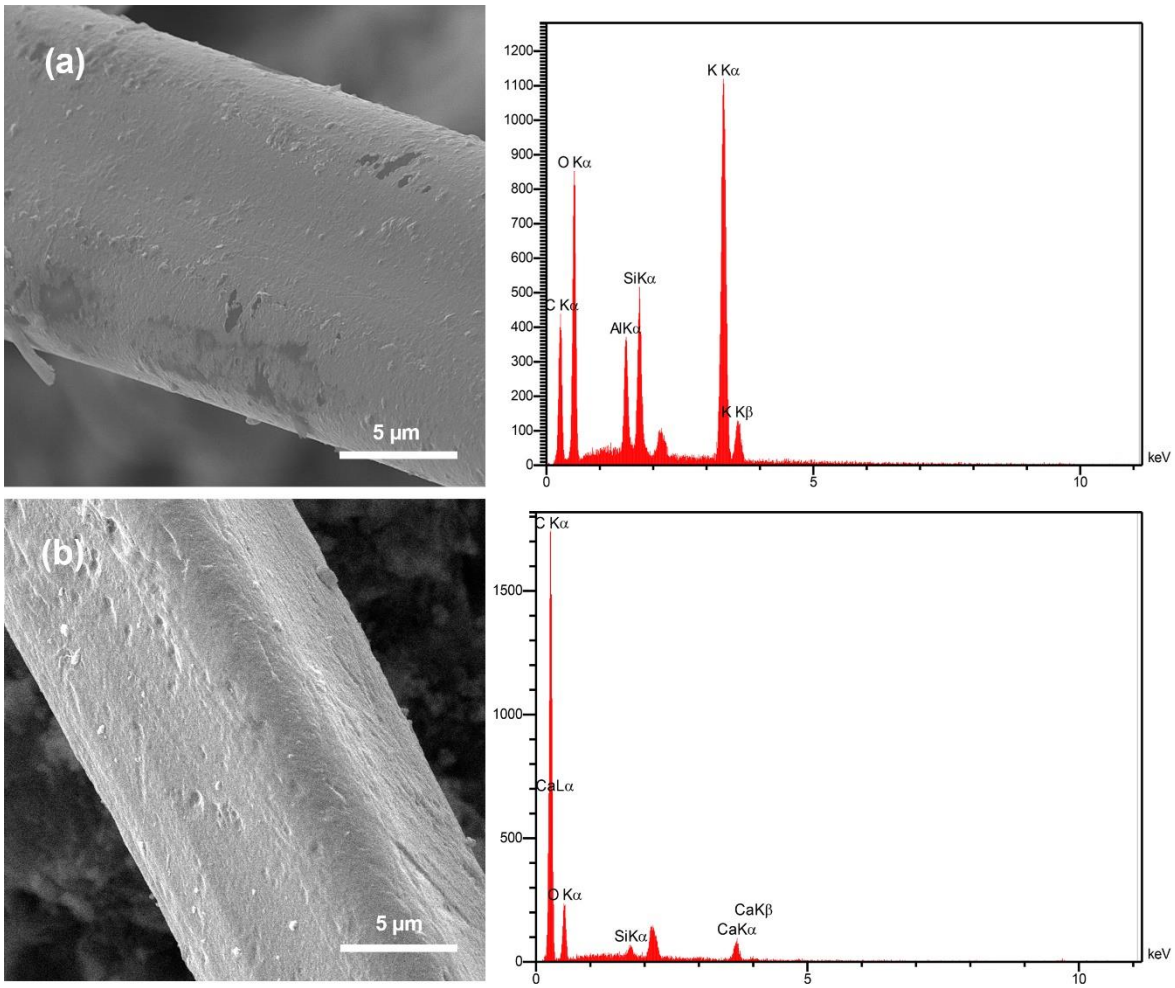

Fig.10. Microstructure of (a) PP fiber in geopolymer matrix and (b) PP fiber in Portland cement matrix with EDX pattern of the surface

Figure 11 shows the microstructure of $GS_{20}F_{0.5}$ and $PS_{20}F_{0.5}$ composites. PP fibers were randomly oriented within both matrices. Almost no fiber agglomeration was observed, and it was evident that the composites exhibited a homogeneous microstructure. The interface between the fiber and geopolymer matrix is shown in Fig. 12(a) with higher magnification. The interfacial bond between the PP fiber and the geopolymer matrix was weak, and an interfacial gap was observed. This suggests that the presence

[DOI: 10.22068/ijmse.4372]

of fibers increased the number of damaging defects in the composites. Consequently, according to Fig. 4, the compressive strength of GS_{20} concrete was higher than that of the $GS_{20}F_{0.5}$ composite, but the concrete failure occurs suddenly and in a brittle manner.

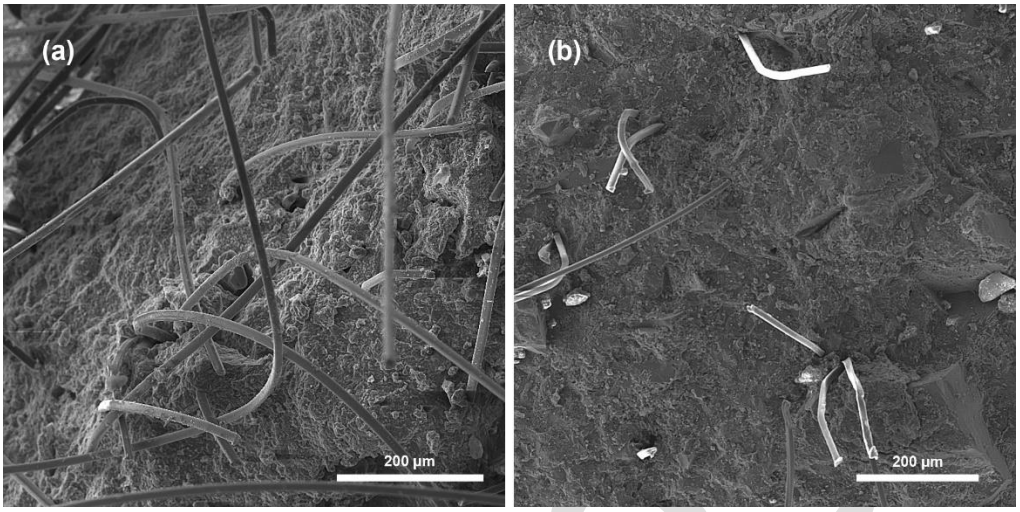

Fig. 11. Fracture surface morphology of (a) geopolymer composite and (b) Portland cement composite

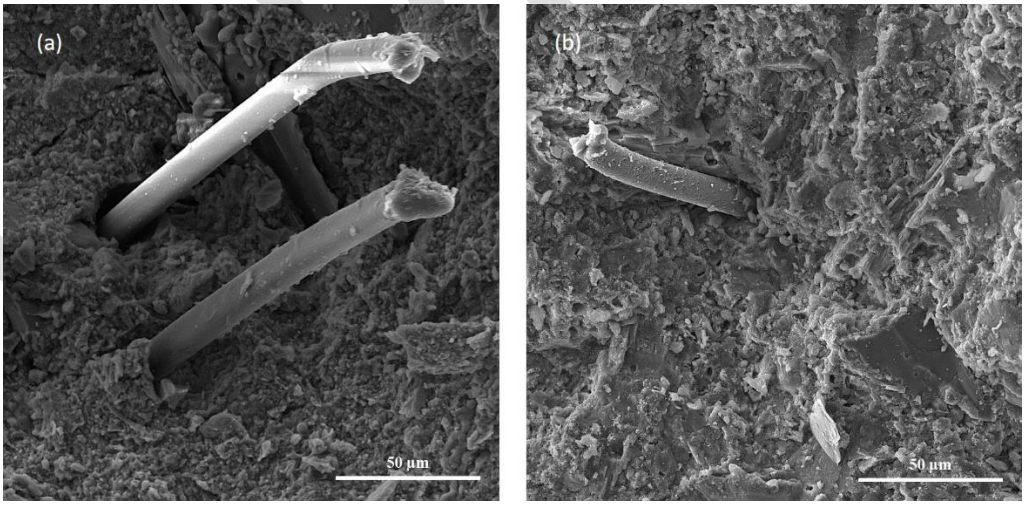

Fig.12. Interfacial microstructure of PP fiber and geopolymer concrete (GS_{20})

As illustrated in Fig. 4, the presence of polypropylene fibers can alter the failure mode from brittle to non-brittle [36], even if they do not have a strong bond with the matrix. This is due to the unique properties of polypropylene fibers, which can resist crack propagation and improve post-peak behavior, even when the bond between the fibers and the matrix is weak. Due to their elastic properties,

[DOI: 10.22068/ijmse.4372]

polypropylene fibers can absorb energy during the loading process. This prevents sudden and brittle failure, allowing the $GS_{20}F_{0.5}$ and $PS_{20}F_{0.5}$ composites to undergo gradual and non-catastrophic deformation under stress. It seems that even if the interfacial bonding is weak, the fibers help absorb and transfer some of the stresses, preventing crack propagation. Considering the strength values and the material's shape, it appears that although the polypropylene fibers are not fully bonded to the matrix, some stresses are still transferred to the fibers, and they act as relative reinforcements. As a result, despite the weak bonding, the fibers can still contribute to changing the material's behavior from brittle to non-brittle failure.

5. Conclusions

This study investigated the microstructural and mechanical performance of metakaolin-based geopolymer composites in comparison with conventional Portland cement composites, with a particular focus on the effects of quartz particle addition and polypropylene fiber reinforcement. The main conclusions are summarized as follows:

1. The geopolymer matrix exhibited a more uniform and denser microstructure compared to Portland cement, which displayed a needle-like, porous, and less compact morphology. This structural difference contributed to the higher compressive strength observed in the geopolymer composites.

2. The incorporation of 20 wt% quartz particles into the geopolymer matrix significantly enhanced mechanical strength and reduced drying shrinkage. In Portland cement composites, quartz particles also improved mechanical performance; however, the reduction in shrinkage was less pronounced due to the participation of water in the hydration reaction.

3. SEM analysis indicated that the interfacial bonding between quartz particles and the geopolymer matrix was more continuous and effective than that in the Portland cement system, resulting in a flexural strength increase approximately 2.5 times greater than that of the corresponding Portland cement concrete.

4. The addition of non-polar polypropylene fibers led to a slight reduction in compressive strength in both geopolymer and Portland cement matrices, primarily due to limited fiber–matrix bonding.

[DOI: 10.22068/ijmse.4372]

However, the fibers significantly enhanced ductility and energy absorption by bridging microcracks, delaying crack propagation, and preventing sudden brittle failure, highlighting a beneficial trade-off between strength and toughness.

5. Overall, the compressive strength of the geopolymer composite was 21.4% higher than that of the Portland cement composite, confirming the superior mechanical efficiency and potential of geopolymer-based materials as durable, ductile, and environmentally sustainable alternatives to conventional Portland cement concretes.

These findings provide valuable insights into the design of fiber-reinforced geopolymer composites with optimized mechanical performance, demonstrating the combined effects of particle reinforcement and fiber addition on strength, ductility, and shrinkage control.

Declarations

Conflict of interest: The authors declare no competing interests.

Financial interests: The authors declare they have no financial interests.

References

1. Duxson, P., Fernández-Jiménez, A., Provis, J.L., Lukey, G.C., Palomo, A. and van Deventer, J.S.J., "Advances in geopolymer science & technology". J. Mater. Sci., 2007, 42, 2917–2933, https://doi.org/10.1007/s10853-006-0637-z.

2. Duxson, P., Provis, J.L., Lukey, G.C. and van Deventer, J.S.J., "The role of inorganic polymer technology in the development of green concrete". Cem. Concr. Res., 2007, 37, 1590–1597, https://doi.org/10.1016/j.cemconres.2007.08.018.

3. Davidovits, J., "Geopolymers: Ceramic-like inorganic polymers". J. Ceram. Sci. Technol., 2017, 8, 335–350, https://doi.org/10.4416/JCST2017-00038.

[DOI: 10.22068/ijmse.4372]

4. Matheu, P.S., Ellis, K. and Varela, B., "Comparing the environmental impacts of alkali activated mortar and traditional Portland cement mortar using life cycle assessment". IOP Conf. Ser.: Mater. Sci. Eng., 2015, 96, 012080, https://doi.org/10.1088/1757-899X/96/1/012080.

5. Barbosa, V.F.F., Mackenzie, K.J.D. and Thaumaturgo, C., "Synthesis and characterisation of materials based on inorganic polymers of alumina and silica: sodium polysialate polymers". Int. J. Inorg. Mater., 2000, 2, 309–317, https://doi.org/10.1016/S1466-6049(00)00041-6.

6. Bakharev, T., "Geopolymeric materials prepared using Class F fly ash and elevated temperature curing". Cem. Concr. Res., 2005, 35, 1224–1232, https://doi.org/10.1016/j.cemconres.2004.06.031.

7. Lyon, R.E., Balaguru, P.N., Foden, A., Sorathia, U., Davidovits, J. and Davidovics, M., "Fire-resistant aluminosilicate composites". Fire Mater., 1997, 21, 67–73, https://doi.org/10.1002/(SICI)1099-1018(199703)21:2.

8. Singh, N.B. and Middendorf, B., "Geopolymers as an alternative to Portland cement: An overview". Constr. Build. Mater., 2020, 237, 117455, https://doi.org/10.1016/j.conbuildmat.2019.117455.

9. Zhang, L., Ahmari, S. and Zhang, J., "Synthesis and characterization of fly ash modified mine tailings-based geopolymers". Constr. Build. Mater., 2011, 25, 3773–3781, https://doi.org/10.1016/j.conbuildmat.2011.04.005.

10. Kuenzel, C., Vandeperre, L.J., Donatello, S., Boccaccini, A.R. and Cheeseman, C., "Ambient temperature drying shrinkage and cracking in metakaolin-based geopolymers". J. Am. Ceram. Soc., 2012, 95, 3270–3277, https://doi.org/10.1111/j.1551-2916.2012.05380.x.

11. Wan, Q., Rao, F., Song, S., Cholico-González, D.F. and Ortiz, N.L., "Combination formation in the reinforcement of metakaolin geopolymers with quartz sand". Cem. Concr. Compos., 2017, 80, 115–122, https://doi.org/10.1016/j.cemconcomp.2017.03.005.

12. Riahi, S., Nemati, A., Khodabandeh, A.R. and Baghshahi, S., "The effect of mixing molar ratios and sand particles on microstructure and mechanical properties of metakaolin-based geopolymers". Mater. Chem. Phys., 2020, 240, 122223, https://doi.org/10.1016/j.matchemphys.2019.122223.

[DOI: 10.22068/ijmse.4372]

13. Samal, S. and Blanco, I., "An application review of fiber-reinforced geopolymer composite". Fibers, 2021, 9, 23, https://doi.org/10.3390/fib9040023.

14. Ranjbar, N., Mehrali, M., Behnia, A., Javadi Pordsari, A., Mehrali, M., Alengaram, U.J. and Jumaat, M.Z., "A comprehensive study of the polypropylene fiber reinforced fly ash based geopolymer". PLoS One, 2016, https://doi.org/10.1371/journal.pone.0147546.

15. Uddin, F. and Shaikh, A., "Tensile and flexural behaviour of recycled polyethylene terephthalate (PET) fibre reinforced geopolymer composites". Constr. Build. Mater., 2020, 245, 118438, https://doi.org/10.1016/j.conbuildmat.2020.118438.

16. Uddin, F. and Shaikh, A., "Review of mechanical properties of short fibre reinforced geopolymer composites". Constr. Build. Mater., 2013, 43, 37–49, https://doi.org/10.1016/j.conbuildmat.2013.01.026.

17. Puertas, F., Amat, T., Fernández-Jiménez, A. and Vázquez, T., "Mechanical and durable behaviour of alkaline cement mortars reinforced with polypropylene fibres". Cem. Concr. Res., 2003, 33, 2031–2036, https://doi.org/10.1016/S0008-8846(03)00222-9.

18. Sahin, F., Uysal, M., Canpolat, O., Cosgun, T. and Dehghanpour, H., "The effect of polyvinyl fibers on metakaolin-based geopolymer mortars with different aggregate filling". Constr. Build. Mater., 2021, 300, 124257, https://doi.org/10.1016/j.conbuildmat.2021.124257.

19. Yazid, M.H., Faris, M.A., Abdullah, M.M.A.B., Ibrahim, M.S.I., Razak, R.A., Nergis, D.D.B., Nergis, D.P.B., Benjeddou, O. and Nguyen, K.S., "Mechanical properties of fly ash-based geopolymer concrete incorporation Nylon66 fiber". Mater., 2022, 15, 9050, https://doi.org/10.3390/ma15249050.

20. Benfratello, S., Palizzolo, L., Sanfilippo, C., Valenza, A. and Ullah, S., "The structural performance of fiber-reinforced geopolymers: A review". Eng., 2025, 6, 159, https://doi.org/10.3390/eng6070159.

21. Blazy, J. and Blazy, R., "Polypropylene fiber reinforced concrete and its application in creating architectural forms of public spaces". Case Stud. Constr. Mater., 2021, 14, e00549, https://doi.org/10.1016/j.cscm.2021.e00549.

[DOI: 10.22068/ijmse.4372]

22. Sokołowska, J.J., Łukowski, P. and Bączek, A., "Mortars with polypropylene fibers modified with tannic acid to increase their adhesion to cement matrices". Appl. Sci., 2024, 14, 2677, https://doi.org/10.3390/app14072677.

23. Shobeiri, F.Z. and Moosavi, A., "Evaluation of properties of chamotte particle-reinforced geopolymer composites in high-temperature applications". J. Aust. Ceram. Soc., 2024, 60, 701–711, https://doi.org/10.1007/s41779-023-00978-5.

24. Tee, K.F. and Mostofizadeh, S., "A mini review on properties of Portland cement concrete with geopolymer materials as partial or entire replacement". Infrastruct., 2021, 6, 26, https://doi.org/10.3390/infrastructures6020026.

25. Taylor, H., "Cement chemistry", second ed. Thomas Telford, London, 1997.

26. Mehta, P.K. and Monteiro, P.J.M., "Concrete: microstructure, properties and materials", fourth ed. McGraw-Hill Education, New York, 2014.

27. Richardson, I.G., "The calcium silicate hydrates". Cem. Concr. Res., 2008, 38, 137–158, https://doi.org/10.1016/j.cemconres.2007.11.005.

28. Nonat, A., "The structure and stoichiometry of C-S-H". Cem. Concr. Res., 2004, 34, 1521–1528, https://doi.org/10.1016/j.cemconres.2004.04.035.

29. Trincal, V., Multon, S., Benavent, V., Lahalle, H., Balsamo, B., Caron, A., Bucher, R., Caselles, L.D. and Cyr, M., "Shrinkage mitigation of metakaolin-based geopolymer activated by sodium silicate solution". Cem. Concr. Res., 2022, 162, 106993, https://doi.org/10.1016/j.cemconres.2022.106993.

30. Lahoti, M., Narang, P., Tan, K.H. and Yang, E.H., "Mix design factors and strength prediction of metakaolin-based geopolymer". Ceram. Int., 2017, 43, 11433–11441, https://doi.org/10.1016/j.ceramint.2017.06.006.

31. Kuenzel, C., Vandeperre, L.J., Donatello, S., Boccaccini, A.R. and Cheeseman, C., "Ambient temperature drying shrinkage and cracking in metakaolin-based geopolymers". J. Am. Ceram. Soc., 2012, 95, 3270–3277, https://doi.org/10.1111/j.1551-2916.2012.05380.x.

[DOI: 10.22068/ijmse.4372]

32. Hajimohammadi, A., Provis, J.L. and van Deventer, J.S.J., "One-part geopolymer mixes from geothermal silica and sodium aluminate". Ind. Eng. Chem. Res., 2008, 47, 9396–9405, https://doi.org/10.1021/ie8006825.

33. Fu, X., Wan, Q., Fan, Y., Zhang, Y., Zhang, R. and Guo, Z., "Impact of altered quartz surface chemistry on mechanical properties and microstructure of geopolymers".Environ. Res., 2025, 285, 122428, https://doi.org/10.1016/j.envres.2025.122428.

34. Kai, M.F. and Dai, J.G., " Understanding geopolymer binder-aggregate interfacial characteristics at molecular level". Cem. Concr. Res., 2021, 149, 106582, https://doi.org/10.1016/j.cemconres.2021.106582.

35. Tome, S., Nana, A., Tchakout´, H.K., Temuujin, J. and Rüscher, C.H., " Mineralogical evolution of raw materials transformed to geopolymer materials: A review". Ceram. Intl., 2024, 50, 35855–35868, https://doi.org/10.1016/j.ceramint.2024.07.024.

36. Korniejenko, K., Lin, W.T. and Šimonová, H., "Mechanical properties of short polymer fiber-reinforced geopolymer composites". J. Compos. Sci., 2020, 4, 128, https://doi.org/10.3390/jcs4030128.

[DOI: 10.22068/ijmse.4372]

Table captions:

Table 1. Chemical composition (XRF) of the metakaolin, microsilica and quartz sand (wt%)

Chemical	SiO_2	Al_2O_3	CaO	Fe_2O_3	TiO_2	MgO	Na_2O	K_2O	SO_3	Cl	C	Si
Metakaolin	53	45	0.09	0.9	0.65	0.03	0.10	0.03	-	-	-	-
Microsilica	96.40	1.32	0.49	0.87	-	0.97	0.31	1.01	0.10	0.04	0.30	0.50
Quartz sand	99.4	0.24	0.09	0.04	-	-	-	-	-	-	-	-

Table 2. Physical and mechanical properties of PP fibers

Fiber	Density (g/cm^3)	Length (mm)	Diameter (□m)	Tensile strength (MPa)	Elongation (%)	Melting temp.(°C)
PP	0.91	6	12	400	80	165

Table 3. Description of Specimens

G (geopolymer)	S_X	S: Quartz sand, X: wt % quartz
	F_Y	F: PP fiber, Y : wt % PP fibers
P (Portland cement)	S_X	S: Quartz sand, X: wt% % quartz
	F_Y	F: PP fiber, Y: wt % PP fibers

[DOI: 10.22068/ijmse.4372]

Table 4. Flexural strengths (MPa) of geopolymer (GS_X) and Portland cement (PS_X) concretes at different quartz sand contents (X, wt%)

Quartz sand (X=)	0	5	10	15	20	25
G	5.62±0.08	7.81±0.13	8.30±0.24	9.14±0.05	15.36±0.11	13.52±0.05
P	3.23±0.21	4.18±0.11	5.87±0.09	6.03±0.21	6.20±0.82	5.49±0.98

Table 5. T-test comparison between geopolymer (GS_X) and Portland cement (PS_X) at each quartz sand content (X, wt%), results are derived from Table 4

X%	GS_X (mean±SD)	PS_X (mean±SD)	t	p-value
0	5.62±0.08	3.23±0.21	23.78	<0.001
5	7.81±0.13	4.18±0.11	47.66	<0.001
10	8.30±0.24	5.87±0.09	21.20	<0.001
15	9.14±0.05	6.03±0.21	32.22	<0.001
20	15.36±0.11	6.20±0.82	24.76	<0.001
25	13.52±0.05	5.49±0.98	18.30	<0.001

Table 6. One-way ANOVA of the effect of quartz sand content (X, wt%) within each binder, values are derived from Table 4

Binder	F	p-value
GS_X	4207.33	<0.001
PS_X	24.59	<0.001

[DOI: 10.22068/ijmse.4372]

Table 7. Flexural strengths (MPa) of geopolymer ($GS_{20}F_Y$) and Portland cement ($PS_{20}F_Y$) composites at different PP fiber contents (Y, wt%)

PP fiber (Y=)	0	0.25	0.5	1	1.25
GS_{20}	15.36±0.11	12.12±0.02	13.11±0.12	11.62±0.14	9.31±0.54
PS_{20}	6.20±0.82	5.03±0.16	4.42±0.08	3.33±0.64	3.15±0.12

Table 8. T-test comparison of flexural strength (MPa) between geopolymer ($GS_{20}F_Y$) and Portland cement ($PS_{20}F_Y$) at each PP fiber content (Y, wt%), values are derived from Table 7

Y%	$GS_{20}F_Y$(mean±SD)	$PS_{20}F_Y$ (mean±SD)	t	p-value
0	15.36±0.11	6.20±0.82	20.44	<0.001
0.25	12.12±0.02	5.03±0.16	44.11	<0.001
0.5	13.11±0.12	4.42±0.08	48.27	<0.001
1	11.62±0.14	3.33±0.64	25.72	<0.001
1.25	9.31±0.54	3.15±0.12	25.01	<0.001

Table 9. One-way ANOVA of the effect of PP fiber content (Y, wt%) on flexural strength within each binder ($GS_{20}F_Y$ and $PS_{20}F_Y$), results are based on the data reported in Table 7

Binder	F	p-value
$GS_{20}F_Y$	88.12	<0.001
$PS_{20}F_Y$	13.45	<0.001

[DOI: 10.22068/ijmse.4372]

Table 10. Effect of quartz sand content (S_X) on the drying shrinkage (%) of geopolymer and Portland cement matrices

Quartz sand (X=)	0	5	10	15	20	25
G	-2.61±0.12	-1.13±0.30	-0.82±0.24	-0.51±0.23	-0.23±0.01	-0.17±0.03
P	-0.24±0.04	-0.23±0.02	-0.13±0.10	-0.09±0.02	-0.06±0.03	-0.04±0.01

[DOI: 10.22068/ijmse.4372]